E. B. Muliawan, S. G. Hatzikiriakos[1], M. Sentmanat*

[1] *Department of Chemical and Biological Engineering, University of British Columbia Vancouver, B.C., Canada*
[2] *Senkhar Technologies, Akron, Ohio, USA*

Melt Fracture of Linear PE

A Critical Study in Terms of Their Extensional Behaviour

In this paper we studied the melt fracture behaviour in capillary flow of a number of polyethylenes produced by various technologies. The critical shear rates for the onset of both sharkskin and gross melt fractures were found to correlate with the high-rate extensional flow behaviour of the polymers. These findings were found to mechanistically support the generally accepted observations of melt fracture occurring at the exit (sharkskin) and entrance (gross) regions of the capillary die. In addition, it was found that boron nitride (BN) behaves as an energy dissipater that suppresses the rapid increase of extensional stress associated with gross melt fracture. This enables BN to act as an effective processing aid in postponing gross melt fracture in the extrusion of polyethylenes.

1 Introduction

Melt fracture is a polymer instability (more pronounced in polyethylenes) that limits the rate of production in many processes such as profile extrusion, film casting, film blowing, blow moulding, and wire coating [1, 2]. In these processes, a polymeric melt emerging from the die often shows surface distortions at throughput rates above a critical value. As a result of these instabilities, the final products become unattractive and commercially unacceptable. This effect can range from loss of gloss of extrudate surface (known also as haziness) to small amplitude periodic distortions (sharkskin melt fracture) and finally to irregular gross distortions (gross melt fracture) at high extrusion rates [3 to 5]. Some of the parameters affecting the degree of extrudate distortion include process temperature, flow rate, concentration and type of additive, geometrical dimensions of the die, chemical nature of the polymer, entrance geometry to the die and many others [3, 5].

There is a general agreement that the site of initiation of sharkskin is located at the die exit [6, 7]. *Howells* and *Benbow* [6] and *Cogswell* [7] hypothesized that polymers fracture at the die exit due to high extensional stresses that develop at this location. The melt leaving the die in the neighborhood of the wall experiences a large, rapid, tensile deformation as the velocity field adjusts from the no-slip boundary condition to the free-surface condition. Polymer chains are stretched during the tensile deformation, which causes the highly entangled polymer to respond like a rubber. The large stresses on the free surface cause periodic cracks that result into small amplitude periodic distortions (sharkskin). This original proposition of fracture at the die exit as the cause of sharkskin has been substantiated by microscopic flow visualization observations reported by *Migler* et al. [8]. The presence of a fluoropolymer at the die exit serves to lubricate the surface of the exiting extrudate thereby reducing the extensional stress transition, resulting in either the complete elimination or postponement of sharkskin to much higher shear rates. Other works supporting the original findings by *Howells* and *Benbow* [6] and *Cogswell* [7] are cited in [9 to 14].

Most authors also agree that above a certain extrusion rate much higher than the critical one for the onset of the exit instability discussed above (sharkskin), the flow upstream of the die contraction becomes unstable. These instabilities occur in the form of sudden pulsation which was confirmed by visualization experiments [15 to 17] and birefringence measurements [18]. The visualization experiments have shown that such instabilities are due to the high elongation stresses that develop at this location of the die. These upstream instabilities cause the phenomenon of gross melt fracture, which is often seen in the form of a regular helix oscillating at the same frequency as that of the pulsations of the upstream elongational flow [15]. Therefore, a critical extensional stress appears to be the criterion for the onset of gross melt fracture [7, 19 to 21]. *Kim* and *Dealy* [21] reported critical extensional stresses for the onset of gross melt fracture of the order of 1 to 2.5 MPa independent of temperature and molecular weight. These values can be significantly higher for polydisperse polymers having a small degree of long chain branching.

As discussed above both sharkskin and gross melt fracture are due to high extensional stresses, their only difference is at the site of their initiation. Therefore, it is logical to study melt fracture phenomena and their relation to the high-rate extensional flow behaviour of polymer melts. However, to measure the extensional rheology of polymers at high rates relevant to the occurrence of melt fracture phenomena was not an easy task to carry out until recently with the development of the SER rheometer [22, 23]. The availability of this unique rheometer has stimulated this work. It is the main objective of this work to study the melt fracture phenomena of a number of polyethylenes and consequently relate their processability to their extensional rheology. This will demonstrate the relevance

* Mail address: S. G. Hatzikiriakos, Dep. of Chem. and Bio. Eng., University of British Columbia, 2216 Main Mall, Vancouver, B.C., Canada VGT 1Z4
E-mail: hatzikir@interchange.ubc.ca

Resin	Commercial nomenclature	Melt index (g/10 min) (I_2)	Density (g/cm^3)	Co-monomer	Catalyst type	Additive	Process technology	Application
A	PF-Y821-BP (LLDPE)	0.80	0.9230	Butene	Z-N	1° + 2° AO, Slip, AB	Unipol Gas Phase	Film
B	TD-9022-D (LLDPE)	0.80	0.9195	Hexene	Z-N	1° + 2° AO, Slip, AB	Unipol Gas Phase	Film
C	FP-120-F (LLDPE)	1.00	0.9218	Octene	Z-N	1° + 2° AO, AB	AST Solution	Film
D	FPs-117-A (LLDPE)	1.00	0.9170	Octene	Single site	1° + 2° AO	AST Solution	Film
E	FP-015-A (LLDPE)	0.55	0.9175	Octene	Z-N	1° + 2° AO, Slip, AB	AST Solution	Film
F	58G (HDPE)	0.95 (I_6)	0.9575	–	Z-N	1° AO	SCLAIR Solution	Blow Molding

Notes: 1° = Primary Anti-Oxidant, 2° = Secondary Anti-Oxidant, AB = Antiblock Agent, Slip = Slip Additive

Table 1. A summary of the molecular characteristics of the polyethylene resins studied

of extensional rheological behavior of polymers in the occurrence of these phenomena and provide additional insight to their origin. Moreover, it is demonstrated that the use of a polymer processing aid (boron nitride), which has been reported to postpone the occurrence of these phenomena at higher shear rates, behaves as an energy dissipater (suppress the rapid development of extensional stresses). Such a finding provides additional evidence as to the existence of a critical extensional stress required for the occurrence of melt fracture.

2 Experimental

Six different polyethylenes were used in this study. The technologies used to produce the resins include gas phase and solution technology using either Ziegler-Natta catalyst or a proprietary single site catalyst developed by Nova Chemicals Corporation. The molecular characteristics of these resins are summarized in Table 1.

Rheological characterization in terms of linear viscoelasticity of all virgin polyethylene samples was performed by using a Rheometrics System IV rheometer equipped with 25 mm parallel plates. The characterization was carried out by performing frequency sweep experiments in the frequency range of 0.01 rad/s to about 500 rad/s. All of the tests were done at temperatures of 170 °C, 190 °C, and 210 °C. Time temperature superposition was applied to obtain the master linear viscoelastic curves at the reference temperature of 170 °C.

The extensional rheology of all virgin resins was assessed with the new SER Universal Testing Platform from Xpansion Instruments [22, 23]. As depicted in Fig. 1 and further described by *Sentmanat* [22, 23], the SER unit is a dual windup extensional rheometer that has been specifically designed for use as a detachable fixture on a variety of commercially available rotational rheometer host platforms. The SER-HV-A01 model used in this study was accommodated on a Rheometrics RDAII rotational rheometer host station platform and was capable of generating Hencky strain rates up to 20 s^{-1} under controlled temperatures in excess of 250 °C. In this work, the extensional rheology of all resins was studied at 170 °C. Extensional melt rheology specimens were prepared by compression molding polymer sample between polyester films to a gage of 0.5 to 1 mm using a hydraulic press. Long polymer strips approximately 15 to 17 mm in width were then cut from the

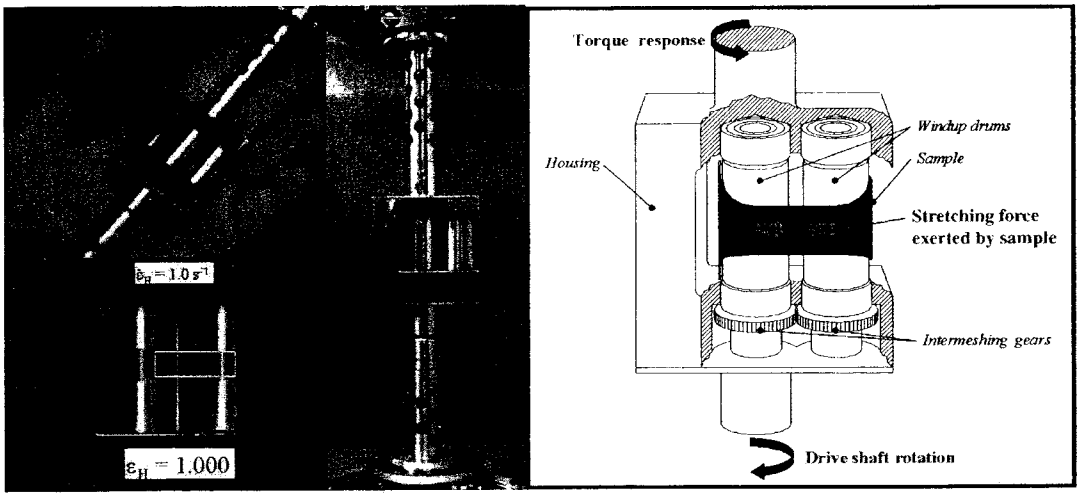

Fig. 1. Universal testing platform accommodated on a rotational rheometer host system, and a schematic illustration of the fixture during operation

molded polymer sheets. From these long strips, individual polymer specimens were then cut to a width of 6.4 to 12.7 mm using a dual blade cutter with an adjustable gap spacing. Typical SER extensional melt rheology specimens range from 40 to 150 mg in mass. Extensional rheology tests began by heating the SER unit to the desired temperature, and after allowing the unit to equilibrate at the temperature, loading and securing the polymer sample onto the preheated drums. Settings for the experiment (e.g. strain rate and frequency of data collection) were input into the software that came with the rotational rheometer.

To examine the processability of polymers in capillary die flow, the Rosand RH-2000 capillary rheometer was used. The barrel was equipped with a three zone electric heater and an adaptive PID temperature controller with an accuracy of 0.1 °C. The barrel was 190 mm in length and 15 mm in diameter. A stepper motor was used to drive the piston from a speed of 0.1 mm per minute to a maximum speed of 600 mm per minute. A pressure transducer installed on top of the piston driver measured the extrusion pressure. The rheometer also came with data analysis software. Only one type of capillary die was used in this study. It was made of tungsten carbide, with a diameter of 1 mm, length to diameter ratio of 16 and entrance angle of 180°. No Bagley correction was applied on the extrusion pressure. The length of the die was considered to be long enough so that the end pressure correction becomes insignificant. During the extrusion process, the piston was allowed to travel down the barrel at a preset speed corresponding to a desired shear rate. The speed was maintained until an obvious steady extrusion pressure was recorded. Polymer samples extruded under steady extrusion pressure were collected. The extruded samples were then inspected by means of both unaided eye and optical microscope to detect the presence of melt fracture.

3 Results and Discussion

3.1 Linear Viscoelasticity

Figs. 2 and 3 show typical master curves of the linear viscoelastic moduli and the complex viscosity of resins A and F respectively, at the reference temperature of 170 °C. This was done by applying the time-temperature superposition which seemed to work very well for all resins examined in this study. Figs. 4, 5, and 6 show the storage modulus, the loss modulus and the complex viscosity functions of all resins at 170 °C. It

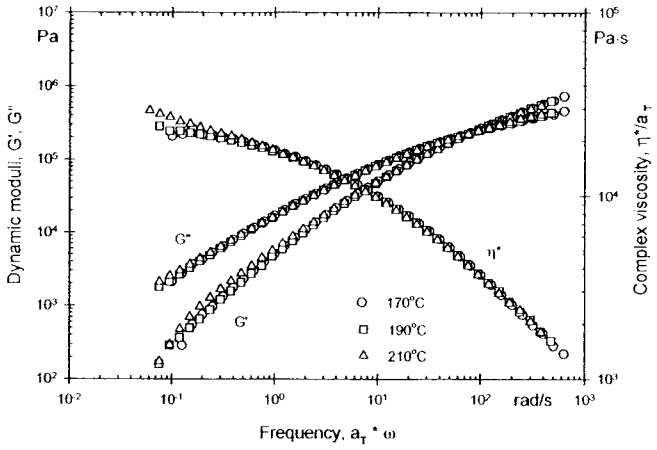

Fig. 2. Master curve of linear viscoelastic properties for resin A

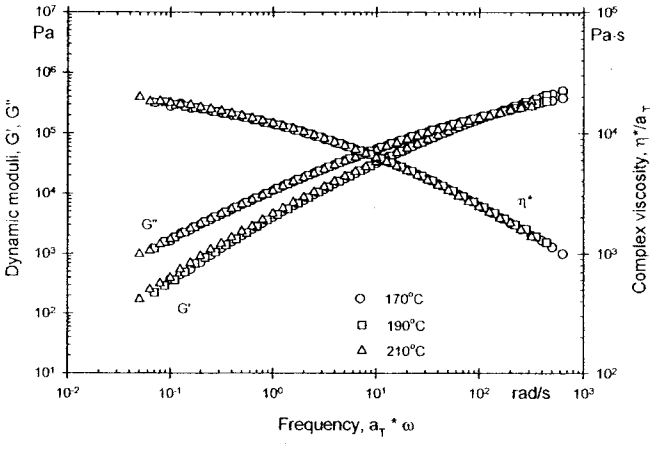

Fig. 3. Master curve of linear viscoelastic properties for resin F

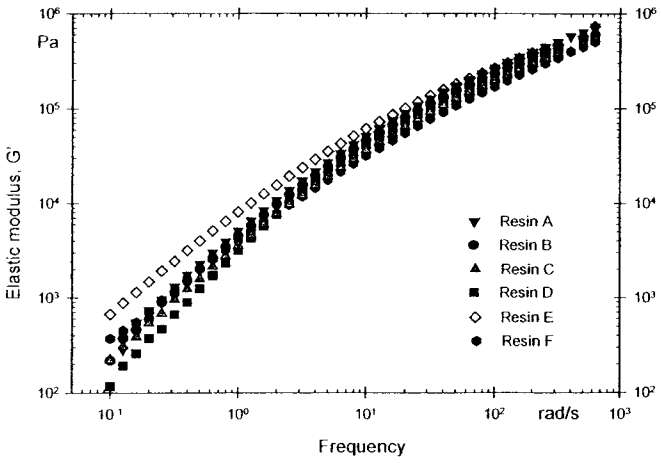

Fig. 4. Elastic moduli of virgin resins A, B, C, D, E and F at 170 °C

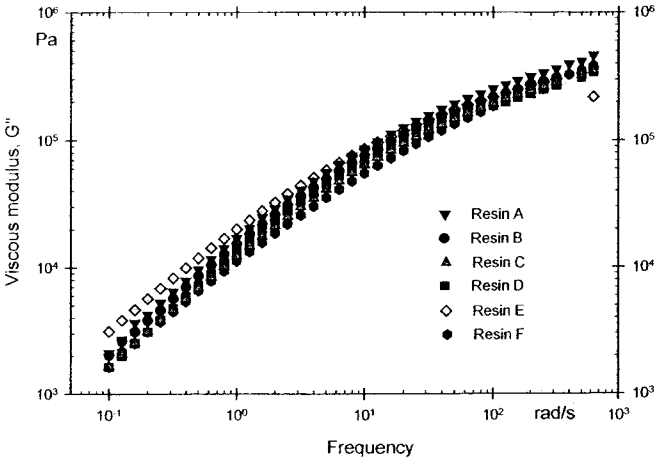

Fig. 5. Viscous moduli of virgin resins A, B, C, D, E and F at 170 °C

can be seen that typically all resins exhibit similar rheological behaviour. Based on such a set of experimental data, very little can be inferred with regard to processability.

The zero shear viscosities for all resins are listed Table 2. These were estimated by fitting the Cross model with the complex viscosity data obtained from the linear viscoelastic experiments. It seems that the zero-shear viscosity correlates well with the melt index data also shown in Table 1.

Resin	η_o (Pa · s)
A	29 100
B	22 700
C	18 363
D	17 728
E	39 198
F	23 256

Table 2. Zero shear viscosities of the resins at 170 °C

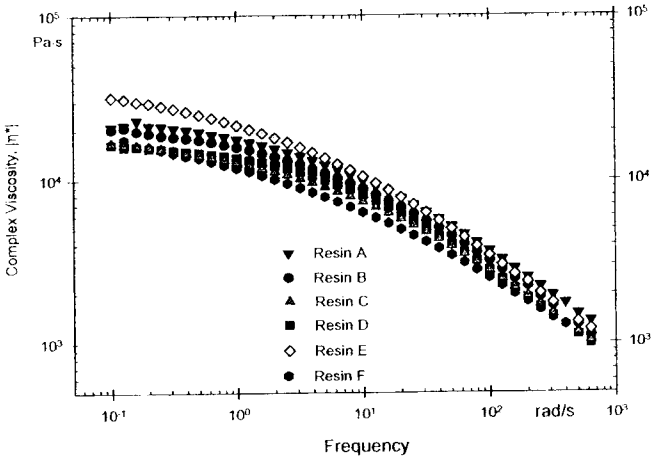

Fig. 6. Complex viscosities of virgin resins A, B, C, D, E and F at 170 °C

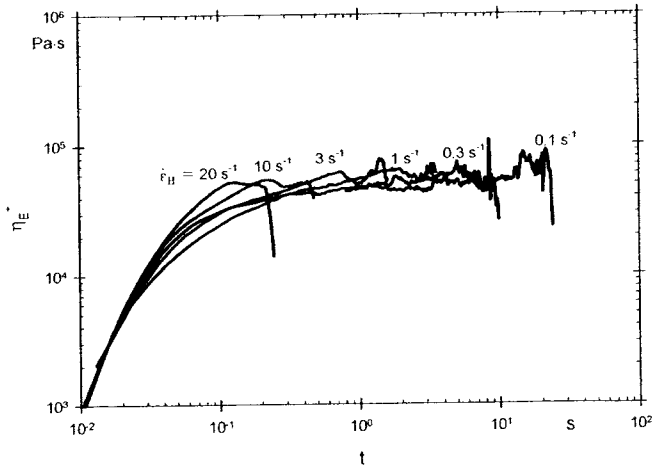

Fig. 7. Tensile stress growth coefficient curves of virgin resin A at 170 °C

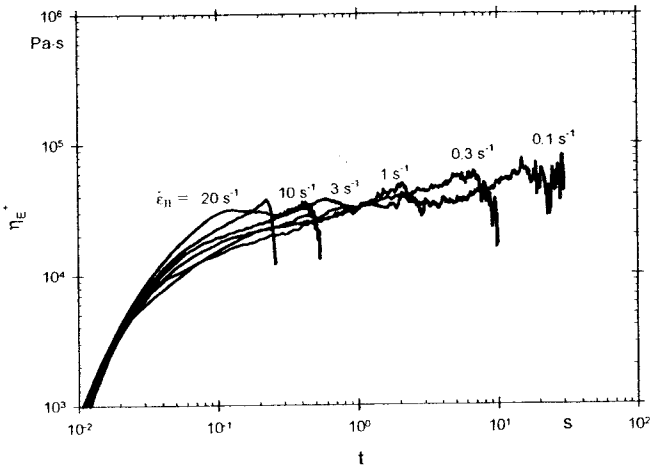

Fig. 8. Tensile stress growth coefficient curves of virgin resin F at 170 °C

3.2 Extensional Rheology

As discussed above the extensional rheology of all the virgin samples was also studied. Typical tensile stress growth coefficient, η_E^+, plots that provide the characterization of the extensional melt flow behavior of the virgin resins A and F are shown in Figs. 7 and 8 respectively. It can be seen that each of these resins exhibits behavior typical for linear polymers. One common characteristic of the extensional behaviour of all resins (including those not shown) is that they exhibit no strain hardening effect. In each of these cases, the tensile stress growth coefficient tends to plateau to a certain level indicated by the linear viscoelastic envelop of each resin before gradually decreasing prior to rupture.

Strain hardening is usually associated with polymers with high molecular weight components and high degree of long branching [24]. With highly branched polymers, for example LDPE, the initial tensile stress growth behavior at low strains is dissipated by the associative flow and deformation behaviour of long chain branches along the polymer backbone. The strain hardening manifested by the significant deviation from linear viscoelastic behavior at large strains is attributed to polymer backbone stretch that is subsequently preceded by polymer melt rupture at much higher deformations. With linear polymers such as the LLDPE and HDPE of this study, although there is little deviation from linear viscoelastic behavior at low rates of extension, at high rates of extension the deformational stresses are borne solely by the polymer chain backbone with little dissipative chain mobility, which leads to melt rupture at lower strains.

3.3 Capillary Extrusion Studies

The processability of the resins was assessed by determining the critical shear rate for the onset of sharkskin and gross melt fractures. All extrusion experiments were carried out at 170 °C over a shear rate range from 10 s^{-1} to 3000 s^{-1} depending on how easily the polymer exhibited melt fracture.

The flow curves obtained from capillary die extrusion experiments are shown in Figs. 9 to 14. Several characteristics common to the processing behaviour of these polymers can be

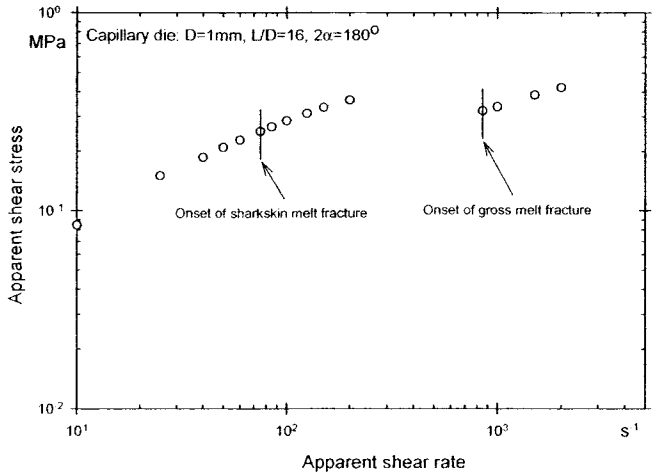

Fig. 9. Flow curves of resin A in capillary die extrusion at 170 °C

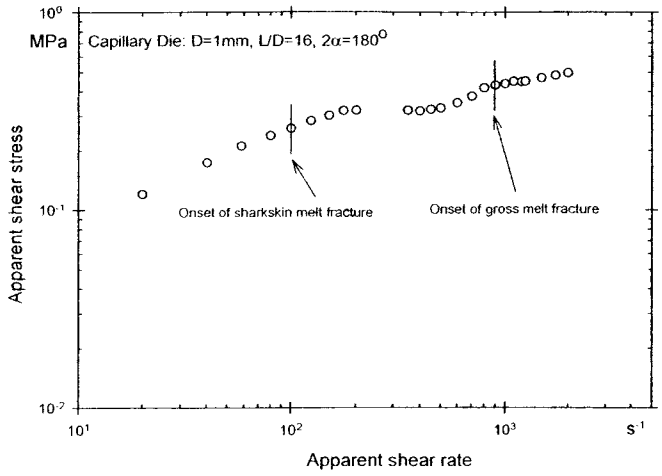

Fig. 10. Flow curves of resin B in capillary die extrusion at 170 °C

seen. First, there is a critical shear stress for the onset of surface/sharkskin melt fracture common to high density and linear low density polyethylenes. At a second critical shear stress and within a range of apparent shear rates the flow becomes unstable a phenomenon known as stick-slip. This stick-slip instability splits the flow curves into two branches, namely a low flow rate and a high flow rate one. At higher rates, the flow becomes again stable; however, the distortions become gross and irregular (onset of gross melt fracture). It is noted that for some resins the onset of gross melt fracture coincides with the beginning of the higher flow rate branch (see Figs. 9 and 12) and for some others there is a delay (see Figs. 10, 11, 13, and 15). In the latter cases, an apparent super-extrusion regime is obtained before the onset of gross melt fracture. The extrudates exhibit minor streaks most of the time when extruded under such conditions.

From the capillary die extrusion data depicted in Figs. 9 to 14, the critical shear rates for the onset of sharkskin, stick-slip and gross melt fractures for all the polymers at 170 °C were determined. These are listed in Table 3. For example, pure resin A exhibits sharkskin melt fracture at a critical shear rate of 75 s^{-1}. This is followed by oscillating flow at 300 s^{-1} and gross melt fracture that occurs at 850 s^{-1}. Most of the resins exhibit similar behaviour, where the critical shear rate for the onset of sharkskin is in the range of 40 to 175 s^{-1}, stick-slip in the range 200 to 600 s^{-1} and gross melt fracture in the range of 700 to 1500 s^{-1}.

As discussed before, the main focus of the present work is the onset of sharkskin and gross melt fractures and their relation to the extensional rheological behaviour. A study on the origin of stick-slip phenomenon and its relation to the extensional rheology of polymers has been reported previously [25]. Since all of the resins exhibited very similar linear viscoelastic behavior, it was concluded that an analysis of the high-rate extensional flow behavior of the resins would provide fundamental insight into their processability due to the fact that tensile melt behavior is believed to play an important role in melt fracture phenomena.

Sample ID		Critical shear rate (s^{-1}) and stress (MPa) for the onset of		
		Sharkskin	Stick-slip	Gross melt
A (LLDPE PF-Y821-BP)	Apparent shear rate	75	300	850
	Apparent shear stress	0.25	0.36	0.32
B (LLDPE TD-9022-D)	Apparent shear rate	100	225	900
	Apparent shear stress	0.26	0.32	0.43
C (LLDPE FP-120-F)	Apparent shear rate	100	325	1100
	Apparent shear stress	0.24	0.36	0.42
D (LLDPE FPs-117-A)	Apparent shear rate	50	600	700
	Apparent shear stress	0.18	0.38	0.38
E (LLDPE FP-015-A)	Apparent shear rate	40	200	700
	Apparent shear stress	0.20	0.34	0.39
F (HDPE 58G)	Apparent shear rate	175	300	1500
	Apparent shear stress	0.26	0.30	0.31

Table 3. Critical shear rates and stresses for all resins in capillary die extrusion at 170 °C

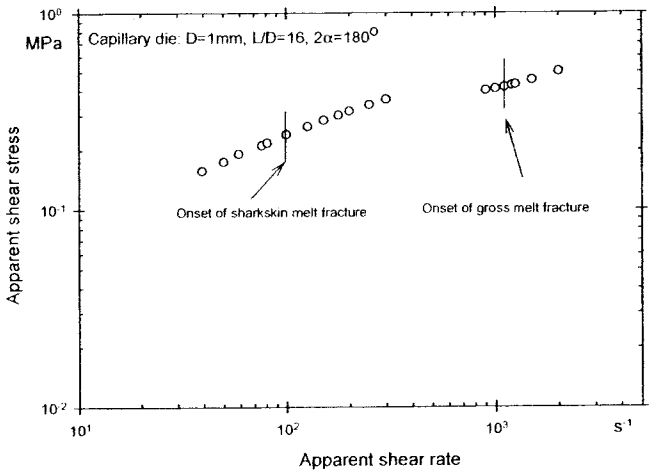

Fig. 11. Flow curves of resin C in capillary die extrusion at 170 °C

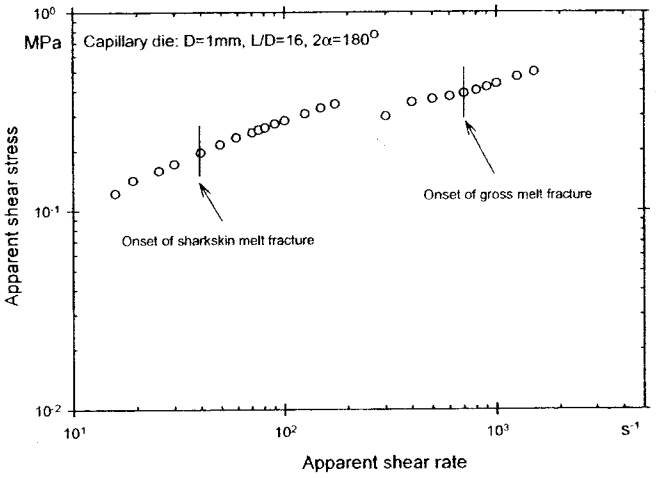

Fig. 13. Flow curves of resin E in capillary die extrusion at 170 °C

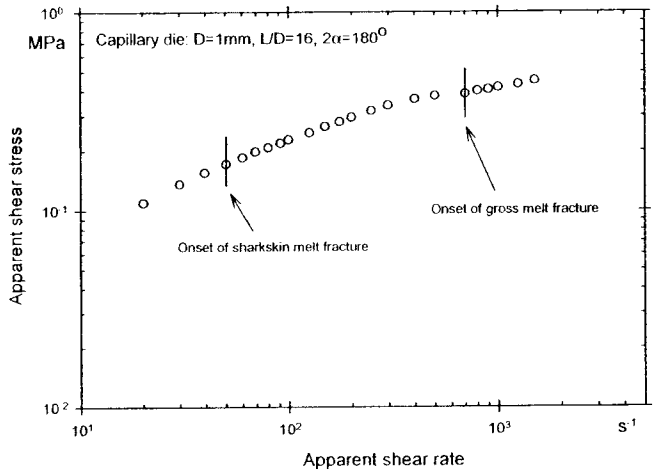

Fig. 12. Flow curves of resin D in capillary die extrusion at 170 °C

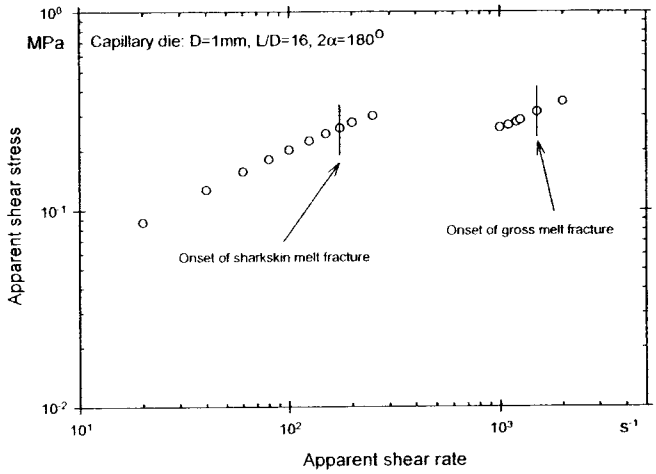

Fig. 14. Flow curves of resin F in capillary die extrusion at 170 °C

3.4 Onset of Sharkskin and Its Relation to Extensional Rheology

As previously described, die exit flow is characterized by a large and rapid increase in elastic tensile stress due to high extensional flow rates on the surface of the extrudate upon exiting the die. Depending on the tensile flow and rupture behavior of a polymer melt, these large extensional stresses may propagate a crack at the melt surface, where the extensional stress is highest, towards the center of the extrudate, where the extensional stress is lowest. This type of sharkskin melt fracture typically occurs at elevated rates of extrusion where the extrudate surface extensional deformation rates are also believed to be high. Fig. 15 contains a plot of true stress versus true strain for all of the polymers at an elevated Hencky strain rate of 20 s^{-1}. It can be seen that resin E exhibits the highest elastic modulus (slope of the curve at the early stages of the extensional deformation), whereas resin F exhibits the lowest. *Sentmanat* et al. [25] recently proposed a mechanistic explanation as to the observation of melt fracture based on the tensile melt flow behavior of linear and highly branched polyethylenes. Based on extensional rheological results at high rates, they have argued that linear polymers exhibit a much steeper rise in tensile stress growth behavior than their highly branched counterparts. They further suggested that the presence of a significant degree of long-chain branching in the bulk polymer acts to retard tensile stress growth to much higher strains due to the dissipative interaction of the polymer branch entanglements prior to the onset of backbone stretch. Furthermore, they asserted that the rapid increase of the extensional stresses in the case of linear polymers leads to rupture of polymers as they exit the die. On the other hand, the tensile retardation mechanism in the case of branched polymers serves to suppress the rapid build up of extensional stress and inhibit crack propagation on the surface of the extrudate. This is mainly the reason that sharkskin is not a problem in the extrusion of branched polyethylenes. Assuming that the die exit phenomena are closely related to the rapidity of elastic energy dissipation within the exiting polymer as has been suggested, the fact that resin E has shown the smallest critical shear rate for the onset of sharkskin melt fracture was not

surprising. On the other hand, resin F exhibited the lowest elastic modulus and as a result fractured (sharkskin) at the highest critical shear rate. In fact, with the exception of resin D, a general correlation exists between the critical shear rate for the onset of melt fracture with the tensile elastic modulus (see critical rates from Table 3 and compare them with the slope of curves from Fig. 15). It can be concluded that the higher the elastic modulus, the smallest the critical shear rate at which sharkskin melt fracture occurs. These experimental results agree well with the trend observed by *Sentmanat* et al. [25].

Resin D has shown an elastic modulus that was similar to that of resin C, however, resin D fractured easier than resin C. This exception could be explained by the fact that resin D was synthesized using a single site catalyst technology, which leads to a narrower molecular weight distribution (typically a polydispersity of about 2) compared to all other polymers, which possess wider polydispersities. Metallocene LLDPE's have been shown to exhibit sharkskin melt fracture at very small shear rates [27]. This in part was related to the low degree of shear thinning behaviour. Compared to all other resins in this study, resin D indeed exhibits the lowest degree of shear thinning. Table 3 also lists the critical shear stress for the onset of sharkskin. While all other resins exhibit sharkskin melt fracture at the critical shear stresses in the range of 0.21 to 0.26 MPa, resin D fractures at 0.19 MPa.

3.5 Onset of Gross Melt Fracture and Its Relation to Extensional Rheology

Another important finding obtained from this study was the relationship between the onset of gross melt fracture with the extensional rheological behaviour of the resins. As discussed above, the extensional deformation undergone by the polymer at the entry region to the die, plays a significant role in the gross melt fracture behaviour of polymers. Rough estimates of average extensional rates at the entrance that correspond to the critical shear rates for the onset of gross melt fracture listed in Table 3, show that the rates are higher than 20 s^{-1} (depending on the resin). Due to limitations with transducer compliance, this rate approaches the upper limit of Hencky strain rate that can be achieved with the SER on commercial rotational rheometer host stations in tensile stress growth mode. In spite of this limitation, it is believed that important conclusions can be made by referring to Fig. 15, which compares the tensile stress, σ_E, of all resins as a function of time at the Hencky strain rate of 20 s^{-1} at 170 °C. It can be seen that all the Ziegler-Natta polyethylenes exhibited an obvious trend; the critical shear rate for the onset of gross melt fracture is inversely correlated with the magnitude of the tensile stress. For example, it can be seen from Fig. 15 that resin E exhibits the highest tensile modulus, which translates to a more rapid increase in extensional stress. The polymer melt reaches its critical extensional stress for the onset of gross melt fracture at an earlier rate. This observation is in agreement with results reported by *Sentmanat* et al. [25]. The only exception that seemed to contradict the correlation between tensile stress and the onset of gross melt fracture was exhibited again by resin D. As described earlier, this was not surprising because resin D was a single site polyethylene, and as such exhibits sharkskin and gross melt fracture at unusually low rates compared to their Ziegler-Natta counterparts.

To further confirm the correlation between tensile stress growth and the onset of gross melt fracture, extensional experiment was performed using a boron nitride (BN)-filled resin (0.1 wt.% of BN CTF5™ supplied by Saint Gobain Advanced Ceramics Corporation was added to the base resin A). It has been shown that certain grades of BN are able to postpone the critical shear rate for the onset of gross melt fracture [28]. Thus, it was expected that BN-filled resin would show reduced tensile stress at Hencky strain rates relevant to gross melt fracture. For this experiment, a model SER-HV-B01 was accommodated on a Bohlin VOR rotational rheometer and it was capable of performing extensional experiment up to a Hencky strain rate of 22.6 s^{-1}. In order to emulate extensional rates closer to those at which gross melt fracture occurs, extensional experiments were performed at a lower temperature of 150 °C. This would also show the dominant effect that BN would have on the onset of gross melt fracture. The tensile stresses for the BN-filled and unfilled resin A at 150 °C are shown in Fig. 16.

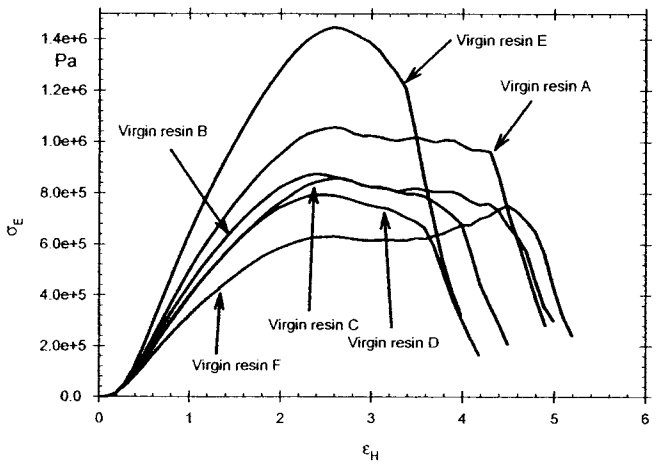

Fig. 15. True tensile stress- Hencky strain curves for all resins at a Hencky strain rate of 20 s^{-1} and temperature of 170 °C

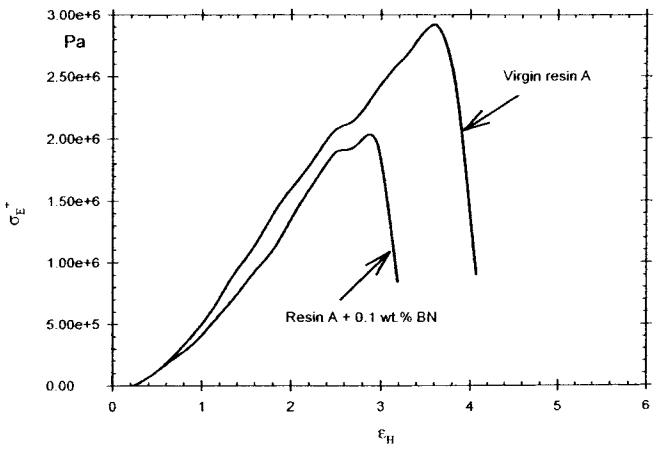

Fig. 16. True tensile stress- Hencky strain curves of BN-filled and unfilled resin A at a Hencky strain rate of 22.6 s^{-1} and temperature of 150 °C

It can be seen clearly that the BN-filled resin showed a significantly lower extensional stress (up to about 30 % lower) compared to the virgin resin. These results demonstrate that BN is able to suppress the increase of extensional stresses that can lead to the initiation of gross melt fracture. Capillary extrusion experiments of this BN-filled resin at 170 °C shows that this BN-filled resin exhibited gross melt fracture at a critical shear rate of 1500 s^{-1}. Note that the virgin resin A showed a critical shear rate for the onset of gross melt fracture at 850 s^{-1}. Thus, the ability of BN to dissipate elastic energy associated with the rapid increase of extensional stresses at high rates of deformation is clearly apparent. In addition, this shows that BN acts as an effective processing aid to postpone the onset of gross melt fracture. This observation is again consistent with the results obtained by *Sentmanat* and *Hatzikiriakos* [26], who performed extensional experiments of BN-filled and unfilled metallocene LLDPE.

4 Conclusions

Six different polyethylenes (five of which are Ziegler-Natta) were used to study the effect of molecular structure on their melt fracture behaviour and subsequently discuss this behaviour in terms of their extensional rheological properties. It was found that the melt fracture behaviour of linear polyethylenes (sharkskin and gross melt fracture) is closely related to high-rate extensional melt rheology. The tensile modulus of the polymer obtained from transient extensional experiments was found to correlate well with the onset of sharkskin melt fracture. On the other hand, the tensile stress was found to be indicative for the onset of gross melt fracture. This was also confirmed by extensional behaviour of boron nitride-filled resin, which showed significant reduction of the tensile stress growth coefficient compared to the unfilled resin.

References

1 *Achilleos, E. C., Georgiou, G., Hatzikiriakos, S. G.:* J. Vinyl and Additive Technology 8, p. 7 (2002)
2 *Ramamurthy, A. V.:* J. Rheol. 30 (2), p. 337 (1986)
3 *Migler, K. B.*, in: Polymer Processing Instabilities: Understanding and Control. *Hatzikiriakos, S. G., Migler, K.* (Eds.), Marcel Dekker, New York (2004)
4 *Georgiou, G.*, in: Polymer Processing Instabilities: Understanding and Control. *Hatzikiriakos, S. G., Migler, K.* (Eds.), Marcel Dekker, New York (2004)
5 *Dealy, J. M., Kim, S.*, in: Polymer Processing Instabilities: Understanding and Control. *Hatzikiriakos, S. G., Migler, K.* (Eds.), Marcel Dekker, New York (2004)
6 *Howells, E. R., Benbow, J. J.:* Trans. Plast. Inst. 30, p. 240 (1962)
7 *Cogswell, F. N.:* J. Non-Newtonian Fluid Mech. 2, p. 37 (1977)
8 *Migler, K., Lavallee, C., Dillon, M., Woods, S., Gettinger, C.:* J. Rheol. 45 (2), p. 565 (2001)
9 *Bergem, N.:* Proceeding 8th Int. Congr. Rheol. Gothenberg, p. 50 (1976)
10 *Piau, J. M., El Kissi, N., Trenblay, B.:* J. Non-Newtonian Fluid Mech. 30, p. 197 (1988)
11 *Vinogradov, G. V., Malkin, A. Y.:* Rheology of Polymers. Mir, Moscow, Springer, Berlin (1980)
12 *Tremblay, B.:* J. Rheol. 35 (6), p. 985 (1991)
13 *Kurtz, S. J.:* Proceeding XIth Int. Congr. on Rheology, Brussels, Belgium, in: Theoretical and Applied Rheology. *Moldenaers P., Keunings R.* (Eds.), Elsevier Science Publishers, Amsterdam (1992)
14 *Moynihan, R. H., Baird, D. G., Ramanathan, R.:* J. Non-Newtonian Fluid Mech. 36, p. 255 (1990)
15 *Piau, J. M., El Kissi, N., Trenblay, B.:* J. Non-Newtonian Fluid Mech. 34, p. 145 (1990)
16 *Kazatchkov, I. B., Yip, F., Hatzikiriakos, S. G.:* Rheol. Acta 39, p. 583 (2000)
17 *Son, Y., Migler, K. B.:* SPE ANTEC Tech. Papers 60, p. 3742 (2002)
18 *Tordella, J. P.*, in: Rheology, *Eirich, F. R.* (Ed.), Academic Press, New York (1969)
19 *Cogswell, F. N.:* Polym. Eng. Sci. 12, p. 64 (1972)
20 *Kim, S., Dealy, J. M.:* Polym. Eng. Sci. 42, p. 482 (2002)
21 *Kim, S., Dealy, J. M.:* Polym. Eng. Sci. 42, p. 485 (2002)
22 *Sentmanat, M. L.:* SER-HV-A01 Universal Testing Platform Instrument Manual. Xpansion Instruments, p. 1-7-1-8 (2003)
23 *Sentmanat, M. L.:* SPE ANTEC Tech. Papers 61, p. 992 (2003)
24 *Münstedt, H.:* J. Rheol. 24 (6), p. 847 (1980)
25 *Sentmanat, M. L., Muliawan, E. B., Hatzikiriakos, S. G.:* Rheol. Acta in press (2004)
26 *Sentmanat, M. L., Hatzikiriakos, S. G.:* Rheol. Acta in press (2004)
27 *Doerpinghaus, P. J., Baird, D. G.:* Rheol. Acta 42, p. 544 (2003)
28 *Hatzikiriakos, S. G.*, in: Polymer Processing Instabilities: Understanding and Control, *Hatzikiriakos, S. G., Migler, K.* (Eds.), Marcel Dekker, New York (2004)

Acknowledgements

This work was financially supported by a strategic grant from NSERC of Canada, STPGP-257907-02.

Date received: October 12, 2004
Date accepted: January 4, 2005